*Human Molecular Genetics, 2007, Vol. 16, No. 9* ***1017–1029***
*doi:10.1093/hmg/ddm047*
*Advance Access published on March 6, 2007*

# Mpp4 is required for proper localization of plasma membrane calcium ATPases and maintenance of calcium homeostasis at the rod photoreceptor synaptic terminals

**Jun Yang[1], Basil Pawlyk[1], Xiao-Hong Wen[2], Michael Adamian[1], Maria Soloviev[2], Norman Michaud[2], Yun Zhao[1,†], Michael A. Sandberg[1], Clint L. Makino[2] and Tiansen Li[1,*]**

[1]The Berman-Gund Laboratory for the Study of Retinal Degenerations and [2]The Howe Laboratory, Department of Ophthalmology, Harvard Medical School, Massachusetts Eye and Ear Infirmary, Boston, MA 02114, USA

Received January 22, 2007; Revised and Accepted February 26, 2007

**Membrane palmitoylated protein 4 (Mpp4) is a member of the membrane-associated guanylate kinase family. We show that Mpp4 localizes specifically to the plasma membrane of photoreceptor synaptic terminals. Plasma membrane $Ca^{2+}$ ATPases (PMCAs), the $Ca^{2+}$ extrusion pumps, interact with an Mpp4-dependent presynaptic membrane protein complex that includes Veli3 and PSD95. In mice lacking Mpp4, PMCAs were lost from rod photoreceptor presynaptic membranes. Synaptic ribbons were enlarged, a phenomenon known to correlate with higher $Ca^{2+}$. SERCA2 (sarcoplasmic-endoplasmic reticulum $Ca^{2+}$ ATPase, type 2), which pumps cytosolic $Ca^{2+}$ into intracellular $Ca^{2+}$ stores and localizes next to the ribbons, was increased. The distribution of $IP_3RII$ ($InsP_3$ receptor, type 2), which releases $Ca^{2+}$ from the stores, was shifted away from the synaptic terminals. Synaptic transmission to second-order neurons was maintained but was reduced in amplitude. These data suggest that loss of Mpp4 disrupts a $Ca^{2+}$ extrusion mechanism at the presynaptic membranes, with ensuing adaptive responses by the photoreceptor to restore $Ca^{2+}$ homeostasis. We propose that Mpp4 organizes a presynaptic protein complex that includes PMCAs and has a role in modulating $Ca^{2+}$ homeostasis and synaptic transmission in rod photoreceptors.**

## INTRODUCTION

The photoreceptors are highly polarized sensory neurons, with their subcellular structures stratified into distinct layers in the retina. In the outermost layer are the outer segments, the elongated organelle that specializes in phototransduction. At the opposite end, the synaptic terminals lie in the outer plexiform layer (OPL). In the dark, photoreceptors are depolarized and L-type $Ca^{2+}$ channels, clustered beneath synaptic ribbons, couple membrane depolarization to $Ca^{2+}$ influx to maintain continuous release of neurotransmitters. Absorption of light by rhodopsin in the outer segment activates the phototransduction cascade leading to closure of the cGMP-gated channels and reduction of sodium influx. The resulting hyperpolarization closes $Ca^{2+}$ channels. PMCAs continue to extrude $Ca^{2+}$ from the synaptic terminals to the extracellular medium (1), and SERCA2 pumps cytosolic $Ca^{2+}$ into the internal stores, the lumen of the endoplasmic reticulum (ER). These coordinated actions lower cytosolic $Ca^{2+}$ and neurotransmitter release ceases. In this way, signals are transmitted from photoreceptors to second-order neurons in the retina (2,3).

Mpp4 is a retina-specific protein (4,5) present at the photoreceptor synapses. There are conflicting reports as to whether it is also present at the connecting cilia, outer limiting membrane or even in other cells of the retina (5–10). Mpp4 belongs to the p55-subfamily of membrane-associated guanylate kinases (MAGUKs). Sequence analysis found L27, PDZ, SH3 and GUK domains (Fig. 1A), all of which are capable of mediating protein–protein interactions. The related protein

*To whom correspondence should be addressed at: Massachusetts Eye and Ear Infirmary, 243 Charles St, Boston, MA 02114, USA. Tel: +1 6175733904; Fax: +1 6175733216; Email: tli@meei.harvard.edu
[†]Present address: Center for Developmental Biology, University of Texas Southwestern Medical Center, Dallas, Texas 75390, USA

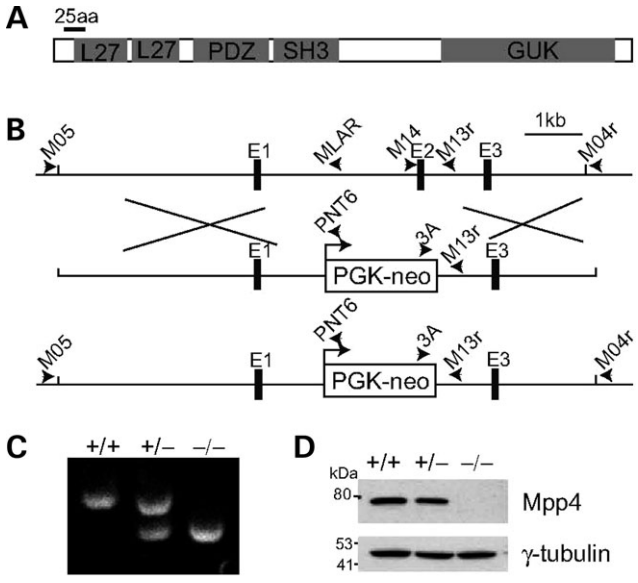


**Figure 1.** Generation of the Mpp4 knockout mice. (**A**) Predicted domain distribution of the Mpp4 protein. L27, lin-2/lin-7; PDZ, postsynaptic density 95/discs large/zonula occludens 1; SH3, src homology 3; GUK, guanylate kinase-like. (**B**) Targeting strategy for disrupting the Mpp4 gene. PCR primers for identification of the mutant and wild-type alleles are shown as arrowheads. M05, MLAR and PNT6 were used for the long arm region. M14, M04r and 3A were used for the short arm region. M14, 3A and M13r were used for routine genotyping during the breeding of Mpp4 mutants. E1, E2 and E3 are exons 1, 2 and 3, respectively. PGK-neo is the neomycin cassette. (**C**) Identification of the mutant allele by genomic PCR using primers M14, 3A and M13r. (**D**) The Mpp4 protein was completely knocked out in the homozygous mutant as shown on an immunoblot. γ-Tubulin is shown as a loading control. +/+, wild-type; −/−, homozygous mutant; +/−, heterozygote.

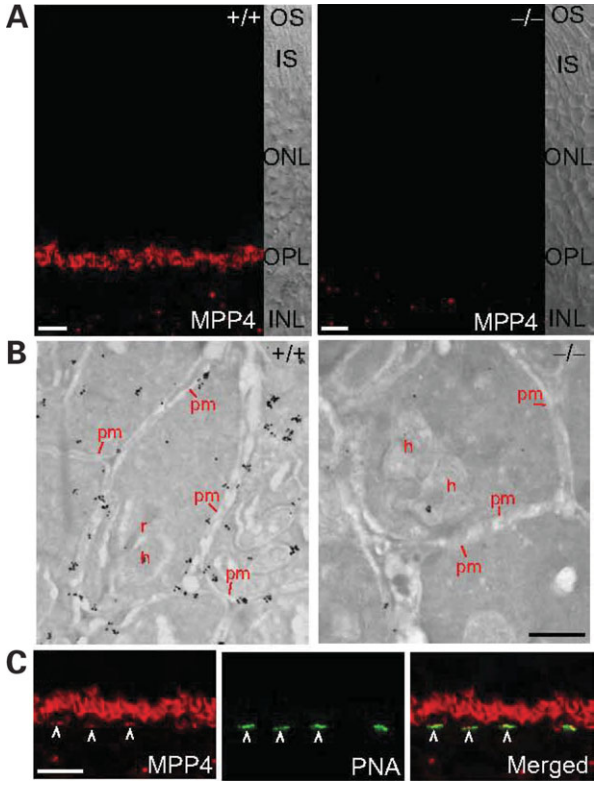


**Figure 2.** Localization of Mpp4 at the rod and cone photoreceptor synaptic terminals. (**A**) Immunostaining of Mpp4 at the OPL. The signals in the INL were non-specific, because they were also present in the Mpp4 knockout mice. OS, outer segments; IS, inner segments; ONL, outer nuclear layer; OPL, outer plexiform layer; INL, inner nuclear layer. (**B**) Immunoelectron microscopy shows that the gold particles labeling Mpp4 were mainly located on the plasma membrane (pm) of the rod terminals. r, synaptic ribbon; h, horizontal cell processes. (**C**) Mpp4 was also present in the cone terminals (arrows), highlighted by peanut agglutinin (PNA) which labels the cones. +/+, wild-type; −/−, Mpp4 mutant. Scale bars, 10 μm (A and C); 500 nm (B).

Mpp5 and Veli3 interact physically with Mpp4 (5,9). In addition, PSD95, Veli3 and Dlg1 are shown to be present in a complex with Mpp4 (10). These data suggest that Mpp4 may function as a scaffolding protein in a multiple-protein complex at the synaptic terminals of photoreceptors.

The physiological function of Mpp4 has remained undefined. No functional deficits were reported in a Mpp4 knockout mouse line (10). In the present study, we generated an independent line of Mpp4 knockout mice and carried out detailed phenotype analyses. We demonstrate that PMCAs associate with the presynaptic membrane protein complex in which Mpp4 is a component, and that gene ablation of Mpp4 leads to loss of PMCAs from the presynaptic membranes, perturbation of $Ca^{2+}$ homeostasis and abnormal synaptic transmission from rod photoreceptors to second-order retinal neurons.

## RESULTS

### Mpp4 protein expression was completely abolished in the Mpp4 knockout mice

$Mpp4^{-/-}$ mice were generated by replacing the second exon of the Mpp4 gene, which contains the translational start codon, with a neomycin cassette (Fig. 1B). The replacement was confirmed by PCR using genomic DNA (Fig. 1C). Mpp4 protein expression was completely abolished in the retina of $Mpp4^{-/-}$ mice as shown by immunoblotting (Fig. 1D). $Mpp4^{-/-}$ mice were viable and appeared comparable with their wild-type littermates in reproductive performance and general health.

### Mpp4 was localized at the synaptic terminals of both rod and cone photoreceptors

Immunostaining in the wild-type retina found Mpp4 at the synaptic layer of the photoreceptors (OPL, Fig. 2A). There were no Mpp4 signals at either the connecting cilium or the outer limiting membrane (Fig. 2A), a finding that differs from previous reports (8–10). As a negative control, staining of $Mpp4^{-/-}$ retinas did not detect signals at the OPL (Fig. 2A). Immunoelectron microscopy revealed that Mpp4 was primarily distributed along the plasma membrane of the photoreceptor synaptic terminals (Fig. 2B). In addition, double staining with Mpp4 and peanut agglutinin, a marker for cone photoreceptors, confirmed the presence of Mpp4 in cone synaptic terminals (Fig. 2C).

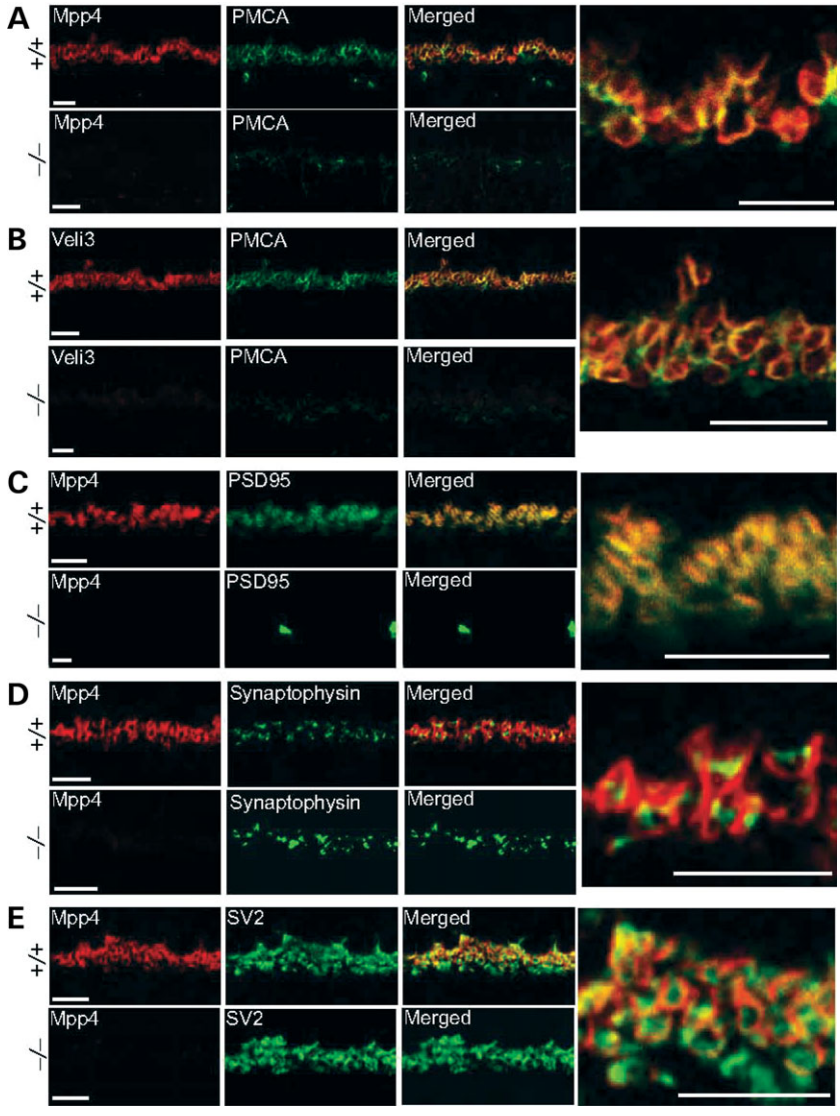


**Figure 3.** Localization of photoreceptor synaptic proteins in the wild-type and the Mpp4 mutant. PMCAs (**A**), Veli3 (**B**) and PSD95 (**C**) co-localized with Mpp4 at the presynaptic plasma membranes of wild-type animals. All were diminished or absent in the Mpp4 mutants. Synaptophysin (**D**) and SV2 (**E**), the synaptic vesicle proteins, were enveloped by Mpp4. Their localizations at the OPL were unaffected in the Mpp4 mutants. The far right column shows higher magnification views of the merged wild-type images. These experiments were carried out using three pairs of retinas from the wild-type and mutant littermates at 9 months of age. +/+, wild-type; −/−, Mpp4 mutant. Scale bars, 10 μm.

### PMCAs interacted with the Mpp4-dependent scaffolding complex at the photoreceptor presynaptic membranes

Four genes code for four PMCA isoforms, and PMCA1, 2 and 4 have been found at the photoreceptor synaptic terminals (11,12). Double immunostaining for Mpp4 and PMCA (all isoforms) suggested their co-localization at the presynaptic membranes (Fig. 3A). PMCA signals were diminished in the Mpp4 mutant as revealed by immunostaining with either a pan-PMCA antibody (Fig. 3A) or a PMCA1 isoform-specific antibody (data not shown). Veli3 and PSD95 were also lost from the synaptic terminals of the Mpp4 mutant (Fig. 3B and C), confirming the observations in an earlier report (10). Double staining for Mpp4 with either synaptophysin or SV2, two synaptic vesicle-associated proteins found them enveloped by Mpp4, consistent with Mpp4 being in the presynaptic plasma membranes (Fig. 3D and E). The signals of synaptophysin and SV2 were unaltered in the mutant.

We studied the interactions among Mpp4, PSD95, Veli3, PMCA1 and PMCA4 by yeast two-hybrid analysis. The b-splicing isoforms of PMCA1 and PMCA4 have a PDZ-binding domain and were used in this analysis. The results (Fig. 4A and B) confirmed the reported interactions of Veli3 with Mpp4 (5), PSD95 with PMCA4b (13), and the reported self-interaction of Mpp4 (9). We also identified novel interactions between Veli3 and PMCA isoforms, and between PSD95 and PMCA1. The interaction of PSD95 with Mpp4 and the interaction of Mpp4 with PMCA4 remain tentative as we detected interaction only in one vector configuration. The interaction between Mpp4 with PSD95 and Veli3 appears to exist

A

| | | ADT7 vector | | | | | |
|---|---|---|---|---|---|---|---|
| | | Mpp4 | Veli3 | PSD95 | PMCA1b | PMCA4b | empty |
| BKT7 vector | Mpp4 | + | ++ | – | – | – | – |
| | Veli3 | ++ | – | – | ++ | ++ | – |
| | PSD95 | + | – | – | + | + | – |
| | PMCA1b | – | + | ++ | – | – | – |
| | PMCA4b | ++ | ++ | ++ | – | – | – |
| | empty | – | – | – | – | – | – |

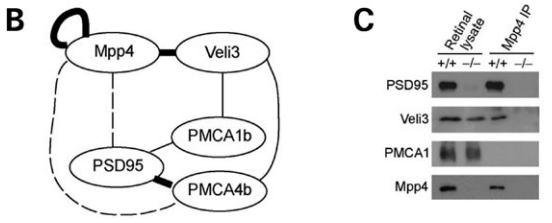


**Figure 4.** Interactions among Mpp4, Veli3, PSD95 and PMCAs in the multiprotein complex of Mpp4. (**A**) The results from yeast two-hybrid protein interaction analyses. ++, strong interaction; +, interaction; −, no interaction. (**B**) A scheme showing the interactions found in the yeast two-hybrid analysis. Thick solid lines denote interactions that were reported previously and were confirmed in this study. Thin solid lines indicate novel interactions found in this study in both vector configurations. Dashed lines indicate tentative interactions that were found in only one vector configuration. (**C**) PSD95 and Veli3, but not PMCA1, were co-immunoprecipitated with Mpp4 from retinal extracts. Mpp4 mutant retinas and a non-specific rabbit IgG protein (data not shown) were used as negative controls. PSD95 was diminished in the Mpp4 mutants indicating this protein was destabilized in the absence of Mpp4. The age of mice used in these experiment was ∼1.5 month. Mpp4 IP, immunoprecipitate using the rabbit Mpp4 antibody. Four percent of total input was loaded in the retinal lysate lanes. +/+, wild-type; −/−, Mpp4 mutant.

*in vivo*, as the latter proteins were detected in Mpp4 immunoprecipitates from retinal homogenates (Fig. 4C). We were unable to detect PMCA1 in the Mpp4 immunoprecipitate, suggesting that their interaction may be transient or indirect.

## Regulators of $Ca^{2+}$ homeostasis were altered in the mutant photoreceptors

Loss of PMCAs from the presynaptic plasma membranes of the mutant photoreceptors suggested that the major $Ca^{2+}$ extrusion mechanism had been compromised. Therefore, we analyzed other known regulators of $Ca^{2+}$ homeostasis in the synaptic terminals of Mpp4 mutant mice. These included the L-type $Ca^{2+}$ channel (14), SERCA2 (15), ryanodine receptors (RyRs) (16) and $IP_3$ receptors ($IP_3$Rs) (17). RyRs and $IP_3$Rs release $Ca^{2+}$ from intracellular stores into the cytosol, whereas SERCAs move $Ca^{2+}$ back into the stores. By immunostaining, SERCA2 was found in a highly restricted location in close proximity to the synaptic ribbons (Fig. 5A and B). Quantitative analysis found that SERCA2 was increased in the photoreceptor terminals of $Mpp4^{-/-}$ mice (Fig. 5C and G). Immunostaining of $IP_3$RII demonstrated that it was located at both the basal outer segments and the synaptic terminals (Fig. 5D and E). The $IP_3$RII immunostaining signal appeared to fill the synaptic terminals (Fig. 5D and E). $IP_3$RII signal intensity in the mutant was increased by 3-fold at the basal outer segments and was decreased by ∼20% at the synaptic terminals (Fig. 5F and G), suggesting a shift in the distribution from the synaptic terminals to the outer segments. $IP_3$R type I ($IP_3$RI) was found primarily in the photoreceptor inner segments and remained unchanged in the mutant (data not shown). The α1F subunit (CACNA1F) is the primary α1 subunit of the L-type $Ca^{2+}$ channel in the rod terminals (18), which forms the channel pore in the membrane. Immunostaining of CACNA1F did not find any obvious changes in the mutant mice, whether they were raised under cyclic lighting or in constant darkness (data not shown). Immunostaining for the three RyRs did not show convincing staining in the photoreceptors but, as a validation of the procedure, did detect signals in extraocular muscles (data not shown).

## Synaptic ribbons were enlarged in the mutant

Histologic examination of eyes from $Mpp4^{-/-}$ mice aged 1−14.5 months did not find apparent retinal degeneration. Mpp4 mutant photoreceptors displayed no abnormality outside of the synaptic layer by electron microscopy (Table 1). Immunostaining for calbindin, a marker for the horizontal cells, found only occasional ectopic horizontal neurites sprouting beyond the synaptic layer and into the photoreceptor nuclear layer (data not shown). Immunostaining for protein kinase Cα, a marker for bipolar cells, did not find ectopic neurites of bipolar cells in the photoreceptor nuclear layer. Therefore, in contrast to several other mutant models with defective synaptic proteins (19−22), $Mpp4^{-/-}$ mice do not develop substantial ectopic neurite sprouting.

The sizes, shapes and densities of rod terminals and synaptic vesicles were indistinguishable between mutant and wild-type mice (Table 1). Bassoon is a scaffolding protein of the presynaptic cytoskeletal matrix assembled at active zones (23). The expanse of Bassoon immunofluorescence was taken as a measure of the synaptic ribbon length. The density of rod synapses was estimated from the number of Bassoon signals per unit area of the OPL. No differences were found between the wild-type and the mutant (Table 1).

The height of the ribbons, measured as the distance between the active zone and the top edge of the ribbon on cross-section electron micrographs, differed substantially between the wild-type and the mutant (Fig. 6A and B). Because synaptic ribbons vary in size under different lighting conditions (24), examinations were carried out under both dark- and light-adapted conditions. Ribbon height was greater in the mutant than in the wild-type under both dark- and light-adapted conditions (Fig. 6C and Table 1). Thus while the length of the ribbons remained similar between mutants and controls, the height of the ribbons increased in the mutant translating into larger-sized ribbons.

## Synaptic transmission from rod photoreceptors to second-order neurons was abnormal in $Mpp4^{-/-}$ mice

Before assessing the functional effects of Mpp4 knockout on synaptic transmission, we sought to determine if phototransduction in the outer segments was altered by recording flash responses of single rods. $Mpp4^{-/-}$ rods were capable of responding (Fig. 7A), although they were unexpectedly more sensitive than normal; they required half as much light to elicit a half-maximal response (Fig. 7B and Table 2). In our

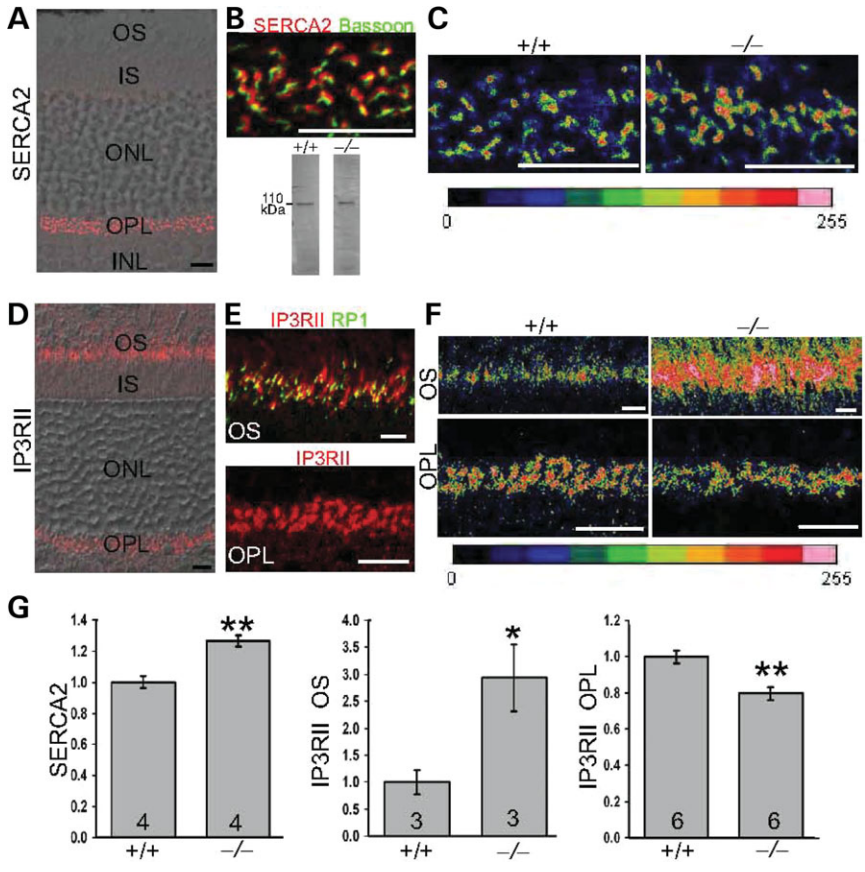


**Figure 5.** Altered expression of $Ca^{2+}$ homeostasis regulators in $Mpp4^{-/-}$ mice. (**A**) SERCA2 immunofluorescence superimposed on a Nomarski image in the wild-type retina. (**B**) SERCA2 (red) localized next to the synaptic ribbons (green) in the rod terminals (upper panel). Lower panel shows immunoblotting with the rabbit SERCA2 antibody on wild-type (+/+) and mutant (−/−) retinal lysates. A protein band of ∼110 kDa was detected. No apparent difference in SERCA2 expression level was seen in the total retinal lysates, which included both photoreceptors and the inner retinal neurons. (**C**) SERCA2 signals in the photoreceptor terminals are shown in pseudo-color. The lookup table is shown below with 0 representing the lowest signal intensity and 255 representing the highest in an 8-bit image. (**D**) $IP_3RII$ fluorescence superimposed on a Nomarski image of a wild-type retina. $IP_3RII$ was present in both the synaptic terminals and the basal outer segments. (**E**) Upper panel: retina doubly stained for $IP_3RII$ (red) and RP1 (green), a marker for the axonemal microtubules in the basal outer segment. Lower panel: $IP_3RII$ distribution at the synaptic terminals. (**F**) $IP_3RII$ signals in the outer segments and the synaptic terminals of both genotypes are shown in pseudo-color, with 0 representing the lowest signal intensity and 255 representing the highest in an 8-bit image. (**G**) The bar charts illustrate changes in the expression of SERCA2 and $IP_3RII$ in Mpp4 mutant photoreceptors. Error bars represent the standard error of the mean. *, $P < 0.05$; **, $P < 0.01$. The numbers in the bottom of each bar indicate the numbers of animals analyzed in each group. Animals examined in this experiment are at the age of 1–3 months. OS, outer segments; IS, inner segments; ONL, outer nuclear layer; OPL, outer plexiform layer; INL, inner nuclear layer. +/+, wild-type; −/−, Mpp4 mutant. Scale bars, 10 μm.

limited sample of rods, the single-photon response of Mpp4 mutants was not significantly larger (Fig. 7C and Table 2). Photon capture and amplification of the phototransduction cascade depend upon intracellular volume (25) but rod outer segment diameter and disk spacing were normal in the mutant rods (Table 1). We attribute the increased sensitivity of photoresponse in the Mpp4 mutant to the 1.9-fold lower expression of rhodopsin kinase (Fig. 7E) and 1.4-fold lower expression of recoverin (Fig. 7F), two proteins that participate in the shutoff of activated rhodopsin. In support of this interpretation, hemizygous rhodopsin kinase knockout rods with reduced expression of rhodopsin kinase are also more sensitive than normal (M. Burns, personal communication). The link between the Mpp4 ablation and decreased levels of rhodopsin kinase and recoverin is not understood, but the adaptive changes to homeostatic regulation of $Ca^{2+}$ in the photoreceptors may offer an explanation (see Discussion). Levels of transducin α-subunit (Fig. 7D), PDE and arrestin (data not shown) were normal. The activity of $Na^+/Ca^{2+}$, $K^+$ exchanger, a $Ca^{2+}$ extrusion mechanism in the outer segments, was also normal (Table 2).

Given that phototransduction remained largely intact in $Mpp4^{-/-}$ rods, we assessed synaptic transmission by electroretinograms (ERGs). ERG a-waves reflect the activity of photoreceptors, and ERG b-waves and oscillatory potentials both reflect the activity of second-order retinal neurons in response to synaptic transmission from photoreceptors. Under dark-adapted conditions that primarily reflect rod activities, the ERG a-wave waveform and amplitude of the Mpp4 mutant were not significantly different from those of the wild-type, consistent with an intact photo-response mechanism in the outer segments (Fig. 8). The ratio of b- to a-wave amplitudes (Fig. 8B) and the amplitude of oscillatory potentials (Fig. 9), however, were significantly decreased in Mpp4 mutants at all ages tested (1, 1.5, 8.5 and 13-months of age; Table 3). The b-wave amplitudes decreased (Fig. 8C) and

**Table 1.** Morphological analysis of rod photoreceptors from the Mpp4$^{-/-}$ mice

| | Wild-type | Mpp4$^{-/-}$ |
|---|---|---|
| Ribbon | | |
| Height, μm | | |
| Dark-adapted | 0.37 ± 0.02, 278, 7 | 0.61 ± 0.03, 307, 7 (0.002) |
| Light-adapted | 0.34 ± 0.01, 211, 7 | 0.47 ± 0.03, 212, 7 (0.02) |
| Length, μm | 1.22 ± 0.03, 104, 2 | 1.23 ± 0.04, 104, 2 |
| Synaptic vesicle | | |
| Size, nm$^2$ | 1059 ± 24, 65, 2 | 1044 ± 28, 60, 3 |
| Density, count per μm$^{-2}$ | 278 ± 13, 11, 2 | 291 ± 15, 17, 3 |
| Spherule | | |
| Size, μm$^2$ | 3.79 ± 0.06, 360, 6 | 3.74 ± 0.07, 316, 6 |
| Density (relative to WT) | 1.00 ± 0.01, 9, 2 | 1.11 ± 0.02, 10, 2 |
| Rod outer segment | | |
| Diameter, μm | 1.36 ± 0.01, 150, 2 | 1.37 ± 0.01, 230, 2 |
| Disk to disk spacing, Å | 314 ± 2, 49, 2 | 320 ± 2, 47, 2 |

Values are given as mean ± SEM, *n*, *N* (*P*). *n* is the number of measurements, and *N* is the number of mice observed. *P*-values are given where significant.

implicit times increased (Fig. 8D) in the mutant. The difference between the mutant and the wild-type was more pronounced at older ages (Fig. 8 and Table 3). Under light-adapted conditions, which isolated the cone responses, the ERG b-waves did not appear to be different (data not shown). Overall, synaptic transmission from rods to second-order neurons was maintained but displayed reduced efficiency as indicated by the lower b-wave amplitudes and oscillatory potentials.

## DISCUSSION

This study demonstrates that Mpp4 is essential for PMCAs to localize to the presynaptic plasma membranes of photoreceptor cells (Fig. 10A). In mice lacking Mpp4, PMCAs were not detected at the photoreceptor synaptic terminals by immunofluorescence, although the proteins were found at normal levels by immunoblotting in retinal extracts. Thus it appears that ablation of Mpp4 disrupts a scaffolding complex and causes PMCA distribution to become randomized throughout the plasma membrane of the cell. Since PMCAs provide the principal means for $Ca^{2+}$ extrusion in photoreceptor synaptic terminals (1,26), their dispersal would raise cytosolic $Ca^{2+}$ in the synaptic terminals of the Mpp4 mutant (Fig. 10B), and impact synaptic transmission. Consistent with this prediction, analysis of the ERG b-waves indicates that synaptic transmission, while still maintained in the mutant, is reduced in efficiency.

Several findings support the view that $Ca^{2+}$ homeostasis was perturbed in the synaptic terminals of the Mpp4 mutant (Fig. 10B). First, expansion of the synaptic ribbons in the mutant suggests a higher cytosolic $Ca^{2+}$. Ribbon size correlates with cytosolic $Ca^{2+}$ in the photoreceptor terminals; ribbons are largest in the dark when $Ca^{2+}$ is high and they shrink in size upon light onset, which decreases $Ca^{2+}$ in the terminals. Furthermore, upon exposure of dissected retinas to EGTA, a $Ca^{2+}$ chelator, the synaptic ribbons also become smaller in size (24). More

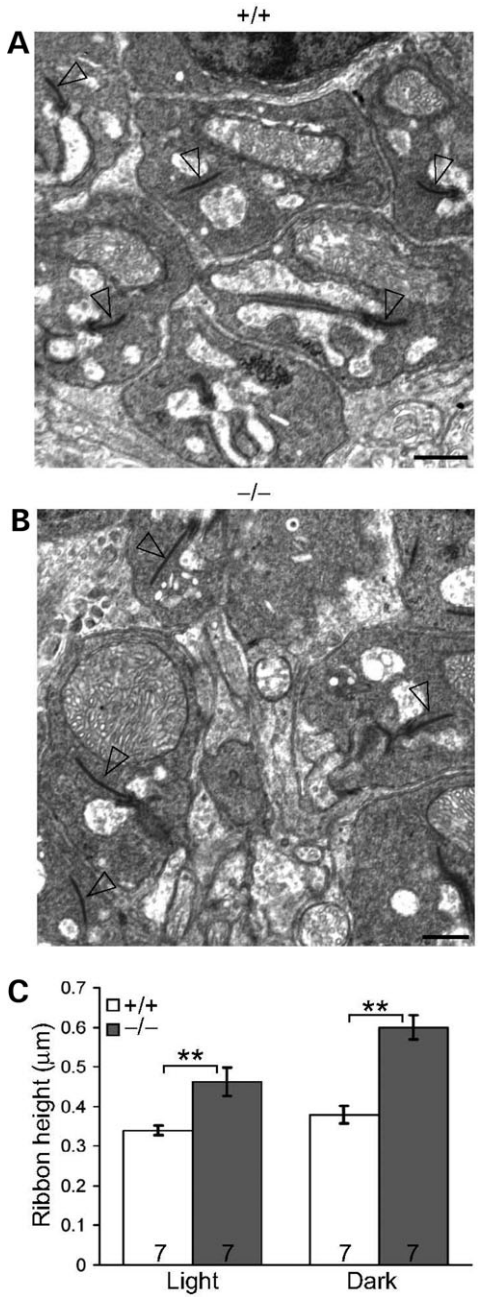


**Figure 6.** Enlargement of the synaptic ribbons in Mpp4 mutant mice. Electron micrographs show that the height of synaptic ribbons (arrowheads) in the rod terminals was greater in the mutant (**B**) than in the wild type (**A**). (**C**) The height of synaptic ribbons was increased in mutants under both light- and dark-adapted conditions. Samples were taken at 3 months of age. Error bars in (C) represent the standard error of the mean. The numbers in the bottom of each bar indicate the numbers of animals analyzed in each group. Scale bars, 500 nm. +/+, wild-type; −/−, Mpp4 mutant. **, statistically significant (see Table 1).

extreme examples of low cytosolic $Ca^{2+}$ in the synaptic terminals are mutant mice lacking key subunits (α1F or α2δ) of the L-type $Ca^{2+}$ channel (20,27,28), which exhibit a near complete absence of synaptic ribbons. These data taken together suggest that ribbon size is a proxy or indicator of cytosolic $Ca^{2+}$ in the synaptic

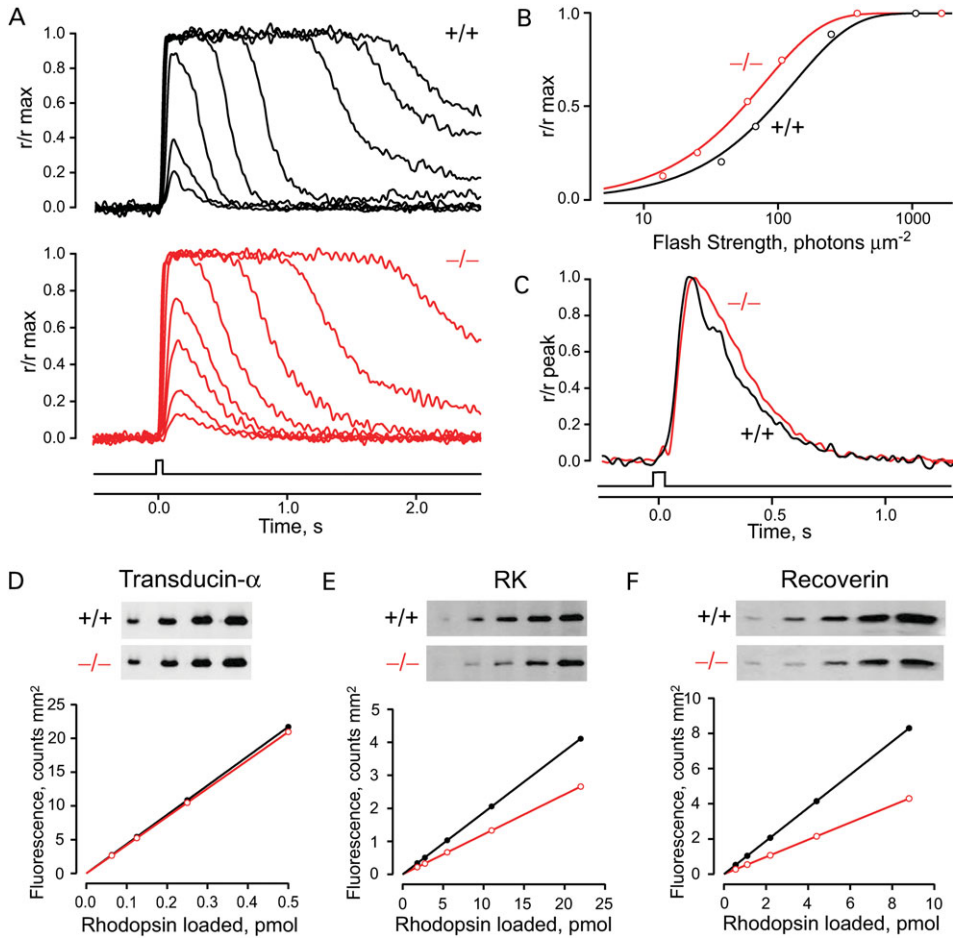


**Figure 7.** Single cell suction electrode recording and assessment of phototransduction protein levels. (**A**) Photoresponses induced by flashes of increasing strength from single cell recordings of two representative rods. Averaged responses were normalized to the maximal response amplitude ($r_{max}$): 7.7 and 8.1 pA for the wild-type (black) and Mpp4 mutant (red), respectively. The flash monitor is shown below. The flash strengths at 500 nm were (photons $\mu m^{-2}$): 38, 68, 250, 1070, 3910, 16700, 33900, 61100 for the wild-type; 14, 25, 59, 107, 391, 1670, 6100, 26100 for the Mpp4 mutant. (**B**) Greater sensitivity of the Mpp4 mutant rod as shown for the rods in (A). Some saturated responses are not shown. The equation, $r/r_{max} = 1 - \exp(-ki)$, was used to fit the results where $r$ is response amplitude, $i$ is flash strength and $k$ is a constant. (**C**) Averaged normalized dim flash responses of 13 wild-type and 16 Mpp4 mutant rods. For each rod, responses with amplitude $<20\%$ of $r_{max}$ were averaged and normalized by the peak amplitude ($r_{peak}$). Assessment of the levels of: (**D**) transducin-α, (**E**) rhodopsin kinase (RK) and (**F**) recoverin in the wild-type rods (black) relative to Mpp4 mutants (red). The relation between specific protein level and total protein loaded (pmoles of rhodopsin loaded) was fit by linear regression. The averaged ratios of the slopes from D–F yielded the amount of protein in the wild-type sample relative to that in the Mpp4 mutant: 1.0, 1.5 and 1.9 for transducin-α ($n = 4$), RK ($n = 4$) and recoverin ($n = 5$), respectively. The animals used for single cell recording and assessment of phototransduction protein levels were wild-type and Mpp4 mutant littermates at 5–8 weeks of age.

terminals. Thus, enlargement of the synaptic ribbons in the Mpp4 mutant is most likely due to an elevated cytosolic $Ca^{2+}$.

Secondly, the altered expression of several $Ca^{2+}$ channels and pumps appears to represent responses from the cell to maintain $Ca^{2+}$ homeostasis. Cytosolic $Ca^{2+}$ is maintained through the concerted actions of $Ca^{2+}$ channels and pumps that localize to plasma membranes or intracellular $Ca^{2+}$ stores. The regulators in turn are tightly regulated at the transcriptional and post-translational levels by $Ca^{2+}$ through a feedback control mechanism (29). An interesting and novel finding of this study is that SERCA2 localizes in close proximity to the synaptic ribbons where vesicle release occurs (Fig. 5). This pool of SERCA2 is significantly increased in the Mpp4 mutant (Fig. 5). The shift of $IP_3RII$ away from the synaptic terminal to the basal outer segment appears to be another adaptive response; less $IP_3RII$ at the synaptic terminals would reduce $Ca^{2+}$ release from the stores. These changes presumably represent an adaptive response of the cell that would lower $Ca^{2+}$ from the cytosol in the synaptic terminals and enhance $Ca^{2+}$ release at distant locales. An intriguing possibility is that removal of $Ca^{2+}$ from the synapse may be effected by ER $Ca^{2+}$ tunneling. $Ca^{2+}$ is taken into the ER where rapid diffusion within the ER lumen (29) allows it to be moved away from the terminals.

Recoverin is a $Ca^{2+}$ binding protein that is present throughout the rod. At the synapse, it may serve as a temporal and spatial buffer for $Ca^{2+}$. Decreased expression of recoverin in the mutant would accelerate the fall in intracellular $Ca^{2+}$ in response to light. Thus altered expression of SERCA2, $IP_3RII$ and recoverin might, to some extent, offset the loss of PMCAs from the synaptic terminals. In the outer segment, rhodopsin kinase and recoverin play a role in the shutoff of

**Table 2.** Flash response characteristics from single cell recordings

| | Wild-type | Mpp4$^{-/-}$ |
|---|---|---|
| $i_{0.5}$, photons $\mu m^{-2}$ | 84 ± 9, 17 | 43 ± 4, 18 (<0.001) |
| Single photon response amplitude, pA | 0.36 ± 0.06, 8 | 0.51 ± 0.07, 16 |
| Dim flash response kinetics | | |
| Time to peak, ms | 132 ± 7, 13 | 147 ± 7, 16 |
| Integration time, ms | 295 ± 31, 13 | 325 ± 14, 16 |
| Recovery time constant, ms | 210 ± 20, 12 | 193 ± 10, 16 |
| $Na^+/Ca^{2+}$, $K^+$ exchanger $\tau_{ex}$, ms | 67 ± 8, 13 | 80 ± 9, 18 |
| Saturating response kinetics $\tau_c$, ms | 252 ± 11, 12 | 241 ± 15, 17 |

Values are given as mean ± SEM, *n* (*P*). *P*-values are given where significant. $i_{0.5}$ is the flash strength needed to elicit a half-maximal photoresponse, hence it is inversely proportional to sensitivity. Single photon response amplitude was calculated by dividing the ensemble variance by the mean dim flash response amplitude. Three parameters were used to describe the kinetics of the dim flash response. Flashes eliciting responses whose amplitudes were <20% of the maximal response were assumed to be dim. Time to peak was measured from mid-flash to the response peak. Integration time was calculated as the integral of the response divided by response amplitude. Recovery time constant was obtained from a fit of the final falling phase of the dim flash response with a single exponential. Bright flash responses that remained in saturation for more than 0.5 s under the least bright flashes were averaged and used to analyze $Na^+/Ca^{2+}$, $K^+$ exchanger. The slow component of the rising phase was fitted with single exponential to determine the time constant of $Ca^{2+}$ extrusion, $\tau_{ex}$ (43). To characterize saturation behavior, the time from mid-flash to 20% recovery of the circulating current was plotted against the natural logarithm of the flash strength. The slope obtained from linear regression, referred to as $\tau_c$, estimates the time constant for the shut-off of transducin (44–46).

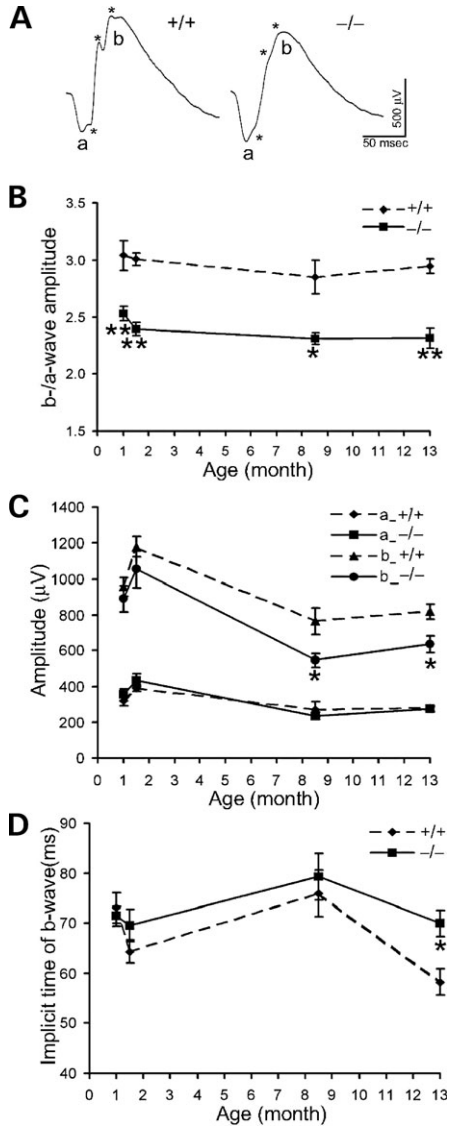


**Figure 8.** Abnormal synaptic transmission from rod photoreceptors to second-order neurons in the Mpp4 mutant. (**A**) Representative dark-adapted ERG tracings from 1 month-old mice showing differences in waveforms, primarily the diminution of oscillatory potentials (*) and the b- to a-wave ratios. (**B**) The ratio of b- to a-wave amplitude was decreased in the Mpp4 mutants at all ages tested. (**C**) The b-wave amplitude was decreased as the mutant animals grew older, whereas the a-wave remained unchanged. (**D**) The implicit time of b-wave was increased in the old Mpp4 mutants. Wild-type and Mpp4 mutant mice used in this experiment were littermates. Error bars represent the standard error of the mean. *, $P < 0.05$; **, $P < 0.01$. +/+, wild-type; −/−, Mpp4 mutant.

rhodopsin. In mutant rods, the increase in rod sensitivity caused by decreased expression of rhodopsin kinase and recoverin could ensure adequate single photon sensitivity in the face of a lowered efficiency of signal transmission at the synapse.

Significant reduction in the dark-adapted ERG b-wave with preservation of the a-wave is a common feature in several mouse models with defects in proteins functioning in signal transmission at the OPL (20–22,27,28,30–35). Compared with those proteins, loss of Mpp4 leads to a milder phenotype. Given our finding that the major $Ca^{2+}$ extrusion pumps are disrupted, one would have expected a more severe synaptic transmission defect. These observations suggest that, compared with PMCA-mediated $Ca^{2+}$ extrusion, SERCA2-mediated $Ca^{2+}$ uptake into the stores is the dominant mechanism of removing $Ca^{2+}$ from the cytosol during rapid synaptic transmission. This view is further supported by the observation that SERCA2 localizes close to the synaptic ribbons, whereas PMCAs, evenly distributed at the plasma membranes, are much further away. The fall in local $Ca^{2+}$ near the synaptic ribbons may be more important for synaptic transmission, despite a higher $Ca^{2+}$ in the larger cytosolic environment of the synaptic terminals of the Mpp4 mutant. As discussed earlier, adaptive responses leading to increased SERCA2 at the ribbon, shifted distribution of $IP_3RII$ and residual PMCAs on the presynaptic membranes may have contributed to the milder phenotype.

The ERG findings in our Mpp4 knockout mice differ somewhat from those in the previously published Mpp4 knockout mouse study, in which ERG abnormalities were not found (10). The large individual variation in the previous study may have precluded detection of relatively small changes. Alternatively, the replacement of different Mpp4 gene fragments and different ERG recording conditions may also provide a partial explanation. Our ERG findings, indicative of abnormal synaptic transmission, are entirely consistent with the mislocalization of PMCAs. Deafwaddler $dfw^{2J}$ mice lack functional PMCA2 protein, which is located at the photoreceptor synaptic terminals and other cells in the retina. These mice have relatively normal cone ERG tracings but their rod

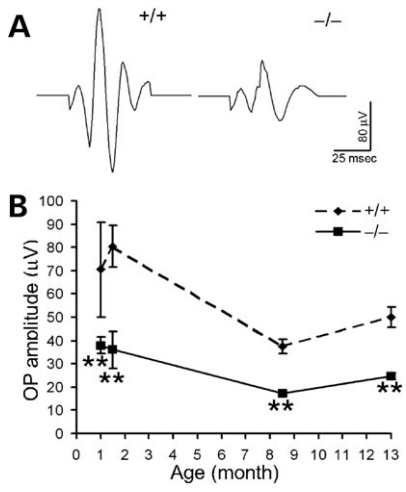


**Figure 9.** Diminished oscillatory potentials in the Mpp4 mutant. (**A**) Representative oscillatory potentials extracted from the ERG tracings in Figure 8A. (**B**) The amplitude of oscillatory potentials was lower in the Mpp4 mutant at all ages tested. Wild-type and Mpp4 mutant mice used in this experiment were littermates. Error bars represent the standard error of the mean. **, $P < 0.01$; +/+, wild-type; −/−, Mpp4 mutant.

ERG b-wave responses are smaller and slower than normal (12). In single cell recordings, rod bipolar cells were less sensitive than normal. In our Mpp4 mutant mice, PMCAs, including PMCA2, were largely lost from the synaptic terminals. Therefore, the Mpp4 mutant phenotype should be inclusive of the rod synaptic terminal defect in the $dfw^{2J}$ mice.

The proximity of the mapped Mpp4 locus with autosomal recessive retinitis pigmentosa 26 (RP26) on human chromosome 2q31–q33 suggested Mpp4 as a possible candidate gene in RP26. Mutation screen of one RP26 family and a panel of 300 unrelated RP patients, however, did not produce any supportive evidence (6). Nor did we find evidence of photoreceptor degeneration in the Mpp4 mutant mice up to 14 months of age, a finding consistent with the study of Aartsen *et al*. (10). Thus it remains an open question as to what type of clinical disease would arise from a defect in Mpp4. It is not known whether the perturbation of $Ca^{2+}$ homeostasis in the synaptic terminals will lead to the eventual demise of the photoreceptors. The role of Mpp4 in cones is another important question that remains to be clarified. If a defect in Mpp4 does underlie some form of human retinal degeneration, the human disease is likely to manifest reduced ERG b-waves and loss of oscillatory potentials at its early stages.

## MATERIALS AND METHODS

### Generation of $Mpp4^{-/-}$ mice

Two genomic fragments (2.8 and 6 kb) flanking the second exon of Mpp4 were amplified from 129/Sv mouse genomic DNA by PCR and inserted as the short and long arms into pGT-N29 vector (New England Biolabs, Beverly, MA) (Fig. 1B). The Mpp4 targeting vector was linearized and electroporated into 129/SvEv embryonic stem (ES) cells. Three ES clones were found to have undergone the correct replacement of the second exon of Mpp4 by the $Neo^r$ cassette, and two of them were separately microinjected into C57BL/6 blastocysts. The resulting chimeras were crossed with C57BL/6 mice, and homozygotes were produced by F1 sibling mating. Heterozygous and homozygous mice were identified with respect to the targeted allele by PCR (Fig. 1B and C). Homozygous mutant mice derived from the two clones did not show any phenotypic difference, hence they were combined for subsequent analyses and data collection. All procedures on animals followed institutional guidelines.

### Antibodies

Mpp4 antibody was raised in rabbit against a recombinant protein encompassing amino acid residues 151–633 of the murine Mpp4 sequence, and was affinity-purified before use. Monoclonal PSD95, calbindin and PKCα antibodies were obtained from Abcam (Cambridge, MA). Monoclonal pan-PMCA, synaptophysin and SERCA2 (clone IID8) antibodies and polyclonal PMCA1 isoform-specific antibody were obtained from Sigma (St Louis, MO). Polyclonal $IP_3RI$, $IP_3RII$ and monoclonal RyR antibodies were obtained from Affinity BioReagents (Golden, CO). Polyclonal Veli3, polyclonal SERCA2, monoclonal SV2 and Bassoon antibodies were purchased from Zymed (South San Francisco, CA), Bethyl Laboratories, Inc. (Montgomery, TX), Developmental Studies Hybridoma Bank (Buckley KM, Harvard Medical School) and Stressgen (Ann Arbor, MI), respectively. The rabbit antibody against CACNA1F was provided by Dr John McRory (University of Calgary, Alberta, Canada). Secondary antibodies conjugated to Alexa fluorochromes and FITC-conjugated peanut agglutinin were obtained from Molecular Probes, Inc. (Eugene, OR). The polyclonal SERCA2 antibody was tested for its specificity by immunoblotting of skeletal and cardiac muscles (data not shown). It recognized a single protein band at ∼110 kDa in both tissues as had been widely reported. In the retina, this antibody recognized a protein at about 110 kDa (Fig. 5B).

### Immunofluorescence, quantitative image analysis and electron microscopy

Eyes were enucleated, placed in fixative and their anterior segments and lens were removed. Fixation continued overnight. The fixative was 4% formaldehyde/PBS in most cases or 2% formaldehyde/0.1% glutaraldehyde/PBS for double labeling of Mpp4 with other proteins. The fixed tissues were soaked in 30% sucrose/PBS for over 3 h, shock frozen and sectioned at 10-μm thick in a cryostat. For antigen retrieval, tissue sections were treated sequentially in Tris (25 mM)/Glycine (200 mM) buffer (pH 7.0) at 80°C for 2 h, hydroxylamine at 80°C for 10 min, sodium borohydride at room temperature for 10 min and 1 mM mercaptoethanol at room temperature for 10 min. For SERCA2 staining, unfixed frozen tissues were sectioned, post-fixed in 4% formaldehyde/PBS for 10 min and permeabilized by 0.2% Triton X-100/PBS for 5 min. Subsequent incubation and washing steps were as described previously (36). Sections were viewed and photographed on a laser scanning confocal microscope (model TCS SP2; Leica).

**Table 3.** ERG analysis

| | 1–1.5 mo Wild-type | Mpp4$^{-/-}$ | 8.5 mo Wild-type | Mpp4$^{-/-}$ | 13 mo Wild-type | Mpp4$^{-/-}$ |
|---|---|---|---|---|---|---|
| a-wave | | | | | | |
| Amplitude, μV | 354 ± 24, 15 | 394 ± 25, 17 | 273 ± 42, 3 | 238 ± 21, 3 | 279 ± 16, 10 | 275 ± 17, 9 |
| Implicit time, ms | 22 ± 1, 15 | 22 ± 1, 17 | 21 ± 1, 3 | 21 ± 1, 3 | 17 ± 0, 10 | 18 ± 0, 9 |
| b-wave | | | | | | |
| Amplitude, μV | 1061 ± 47, 15 | 968 ± 64, 17 | 765 ± 74, 3 | 547 ± 39, 3 (<0.05) | 819 ± 43, 10 | 637 ± 47, 9 (<0.05) |
| Implicit time, ms | 69 ± 2, 15 | 71 ± 2, 17 | 76 ± 5, 3 | 79 ± 5, 3 | 58 ± 3, 10 | 70 ± 3, 9 (<0.01) |
| $b_{Amp}/a_{Amp}$ | 3.03 ± 0.07, 15 | 2.47 ± 0.05, 17 (<0.001) | 2.85 ± 0.15, 3 | 2.31 ± 0.05, 3 (<0.05) | 2.95 ± 0.07, 10 | 2.32 ± 0.09, 9 (<0.001) |
| OP | | | | | | |
| Amplitude, μV | 78 ± 8, 7 | 37 ± 5, 7 (<0.001) | 38 ± 3, 3 | 17 ± 1, 3 (<0.01) | 50 ± 4, 8 | 25 ± 1, 6 (<0.001) |
| Frequency, Hz | 59 ± 1, 7 | 56 ± 3, 7 | 62 ± 2, 3 | 50 ± 5, 2 | 60 ± 2, 7 | 58 ± 2, 6 |

Values are given as mean ± SEM, *N* (*P*). *N* is the number of animals analyzed. *P*-values are given where significant.

Image data were acquired from wild-type and Mpp4 mutant tissues under identical conditions that produced only a few saturated pixels, and were analyzed quantitatively using the image processing program, ImageJ 1.34s (NIH). Three regions along the vertical meridian (two at the periphery and one close to the optic nerve) were measured and averaged for each tissue section. Three or four tissue sections were measured and averaged for each animal. For each group, three to six animals were analyzed. Because SERCA2 signals appeared as discrete horseshoe-shaped particles at the OPL, we measured their intensity using the 'analyze particles' function of ImageJ and averaged the intensities of the particles in each region for one measurement. To measure the intensities of $IP_3RII$ and CACNA1F signals, we manually circled their signals at the OPL ($IP_3RII$ and CACNA1F) and the outer segments ($IP_3RII$) and used the 'measure' function of ImageJ. To remove the background, the intensities measured immediately outside the area of positive $IP_3RII$ signal at the outer segments were subtracted. Transmission electron microscopy and immunoelectron microscopy were carried out as previously described (36).

### Yeast two-hybrid, immunoprecipitation and immunoblotting analyses

Mouse Mpp4 (GenBank accession no. NP_660125), Veli3 (GenBank accession no. NP_035829), PSD95 (GenBank accession no. NP_031890) and C-terminal fragments of PMCA1b (amino acid 1110–1220, GenBank accession no. NP_080758) and PMCA4b (amino acid 1097–1205; GenBank accession no. NP_998781) were PCR amplified from retina cDNAs, and cloned into pGADT7 and pGBKT7 vectors. Yeast two-hybrid analysis was performed as described previously (36).

Retinas were dissected from six wild-type and six mutant mice at the age of 5 weeks. The tissues were homogenized and incubated for 30 min in a lysis buffer (50 mM Tris–HCl pH8.0, 150 mM NaCl, 0.5% Triton X-100, 5 mM EDTA, 0.5 mM PMSF, 1X protease inhibitor and 1 mM DTT). They were then incubated with protein G sepharose (Amersham Biosciences, Piscataway, NJ) for 1 h and centrifuged at 18 000*g* for 10 min to remove non-specific precipitates. The supernatants were incubated with the primary antibody for 3 h and then centrifuged at 18 000*g* for 10 min. The resulting supernatants were incubated with protein G sepharose for an additional hour. After a brief centrifugation at 2000*g*, the pellets were washed with the lysis buffer four times and then boiled in Laemmli protein sample buffer. All incubation and centrifugation procedures were performed at 4°C. A non-immune rabbit IgG served as a negative control. Immunoblotting and protein quantification were carried out as described previously (36,37). To perform immunoblotting of SERCA2, two retinas were sonicated in 500 μl of $H_2O$ and solubilized in Laemmli protein sample buffer. The samples were loaded on SDS–polyacrylamide gels without boiling (to avoid formation of rhodopsin aggregates).

### Quantitative morphologic assessment of the rod photoreceptors

The synaptic ribbons in the rod synaptic terminals are tethered to the arciform densities via a cytomatrix protein complex in which the protein Bassoon is a component (22). Immunofluorescence staining for Bassoon gave discrete crescent-shaped objects in rods, which were measured as representing synaptic ribbon length in the *en face* view. The Bassoon signals from cone synaptic terminals were distinct from rods and excluded in this assessment. The individual measurements of synaptic ribbon length were normalized to the wild-type average prior to statistical analysis. The density distribution (number of discrete crescent-shaped objects per unit area in the OPL) was taken to represent the density distribution of rod synaptic terminals. On electron micrographs, the height of synaptic ribbons, the size and density distribution of synaptic vesicles

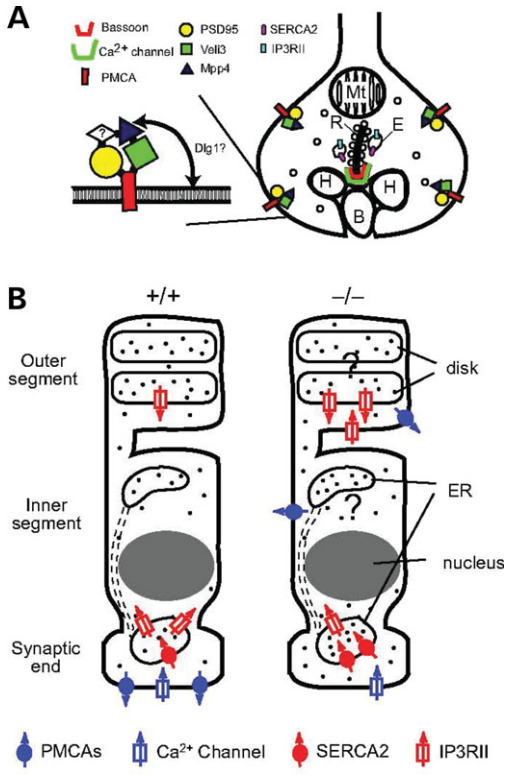


**Figure 10.** A model for Mpp4 function in the rod photoreceptor synaptic terminal. (**A**) Mpp4 mediates the formation of a protein complex at the presynaptic membrane of the photoreceptor synaptic terminal, which includes PSD95, Veli3 and PMCA (left). This complex is required for the correct localization of PMCAs at the presynaptic membranes as has been demonstrated in the present study. Dlg1 may be involved in anchoring this complex to the presynaptic membrane (10). The Mpp4 multi-protein complex is physically separate from the synaptic ribbons; it does not interact directly with the synaptic ribbon and ribbon-associated proteins (right). Mt, mitochondrion; R, synaptic ribbon; E, endoplasmic reticulum; H, horizontal cell process; B, bipolar cell dendrite. (**B**) Cytosolic $Ca^{2+}$, represented by small black dots, is increased at the synaptic terminals because of insufficient extrusion. The $Ca^{2+}$ increase originated at the terminal is likely to spread out throughout the cell facilitated by, for example, ER $Ca^{2+}$ tunneling. The change in $Ca^{2+}$ concentration in the inner and outer segments is unknown but the upregulation of $IP_3RII$ in the basal outer segments suggests an altered state of $Ca^{2+}$ flux. +/+, wild-type; −/−, Mpp4 mutant.

and the size of synaptic terminals were measured. Ribbon height was measured from the arciform density to the tip of the ribbon, i.e. the distance the ribbon jutted into the cytoplasm. Twenty to 50 ribbons were measured in each eye. One eye was measured from each animal. In total, seven animals were analyzed in each group. Statistical analysis was carried out based on seven animals with 20–50 repetitive measurements. Because ribbon height was reported to fluctuate during a 24-h diurnal cycle and differ between black and albino C57BL/6J mice (38,39), we compared ribbon height between the Mpp4 knockout and wild-type mice, all of which had agouti coat color, at the same time point during a day. Eyes were enucleated from mice that were dark-adapted overnight (dark-adapted) and from mice that were dark-adapted followed by light adaptation for 1 h (light-adapted). The measurements were carried out using ImageJ 1.34s (NIH). Morphologic assessment of rod outer segments was carried out as previously described (37).

### ERGs and single-cell suction electrode recording

ERG recording was performed as described previously (40). To measure oscillatory potentials, we quantified the mean absolute amplitude and plotted the waveform between the trough of the a-wave and peak of the b-wave in the time domain after a 30 Hz high-pass filter and quantified peak amplitudes in the frequency domain by fast Fourier transform following a Blackman window (41). For single-cell suction electrode recording, three Mpp4 knockout and five wild-type control mice at 5–8 weeks of age were used following a protocol as described previously (42). Briefly, mice were dark-adapted overnight. Retinas were dissected and chopped under infrared light. The tissue was then maintained at 37°C in a recording chamber and perfused constantly with an enriched bicarbonate buffered Ringer's solution equilibrated with 95% $O_2$/5% $CO_2$. The outer segment of a rod was sucked into a silanized glass electrode. The electrode was filled with (mM): 140 $Na^+$, 3.6 $K^+$, 2.4 $Mg^{2+}$, 1.2 $Ca^{2+}$, 145.8 $Cl^-$, 10 HEPES, 0.02 EDTA and 10 glucose (pH 7.4). Rods were stimulated with light from a xenon arc source passing through a 6 cavity interference filter (500 nm, Omega Optical, Brattleboro, VT) and neutral density filters. A 23 ms flash was used for all experiments. Photocurrent was measured with an Axopatch 200A amplifier (Axon Instruments, Union City, CA), filtered at 30 Hz (−3 dB, 8-pole Bessel, Frequency Devices, Haverhill, MA) and digitized at 400 Hz by Pulse/PulseFit (version 8.07, HEKA Elektronik, Germany). The delays introduced by filtering were not corrected. Data were analyzed off-line by Igor Pro (version 5.03, WaveMetrics, Inc., Lake Oswego, OR) with 12 Hz digital filtering.

### Statistical analysis

Persons performing quantitative measurements in most instances were masked with regard to the genotypes. To compare the measured values for control and Mpp4 knockout mice, we used the Student's *t*-test when there were single values per animal and PROC GENMOD of SAS, version 9.1 when there were multiple values per animal. A *P*-value of less than 0.05 was considered to indicate statistical significance.

## ACKNOWLEDGEMENTS

We thank Dr John McRory (University of Calgary, Alberta, Canada) for the gift of the CACNA1F antibody, Akella Sreedevi for histologic preparations and Drs E.L. Berson, C.W. Morgans, O. Bulgakov, X. Sun and X. Liu for their helpful suggestions. This work was supported by National Institutes of Health grants EY10309 (TL), EY12944 (CLM), NIH Core Grant for Vision Research EY14104 and the Foundation Fighting Blindness.

*Conflict of Interest statement*. None declared.

## REFERENCES


1. Morgans, C.W., El Far, O., Berntson, A., Wassle, H. and Taylor, W.R. (1998) Calcium extrusion from mammalian photoreceptor terminals. *J. Neurosci.*, **18**, 2467–2474.
2. Morgans, C.W. (2000) Neurotransmitter release at ribbon synapses in the retina. *Immunol. Cell Biol.*, **78**, 442–446.
3. Krizaj, D. and Copenhagen, D.R. (2002) Calcium regulation in photoreceptors. *Front. Biosci.*, **7**, d2023–d2044.
4. Stohr, H. and Weber, B.H. (2001) Cloning and characterization of the human retina-specific gene MPP4, a novel member of the p55 subfamily of MAGUK proteins. *Genomics*, **74**, 377–384.
5. Stohr, H., Molday, L.L., Molday, R.S., Weber, B.H., Biedermann, B., Reichenbach, A. and Kramer, F. (2005) Membrane-associated guanylate kinase proteins MPP4 and MPP5 associate with Veli3 at distinct intercellular junctions of the neurosensory retina. *J. Comp. Neurol.*, **481**, 31–41.
6. Conte, I., Lestingi, M., den Hollander, A., Miano, M.G., Alfano, G., Circolo, D., Pugliese, M., Testa, F., Simonelli, F., Rinaldi, E. *et al*. (2002) Characterization of MPP4, a gene highly expressed in photoreceptor cells, and mutation analysis in retinitis pigmentosa. *Gene*, **297**, 33–38.
7. Li, M., Zhang, S.S. and Barnstable, C.J. (2003) Developmental and tissue expression patterns of mouse Mpp4 gene. *Biochem. Biophys. Res. Commun.*, **307**, 229–235.
8. Stohr, H., Stojic, J. and Weber, B.H. (2003) Cellular localization of the MPP4 protein in the mammalian retina. *Invest. Ophthalmol. Vis. Sci.*, **44**, 5067–5074.
9. Kantardzhieva, A., Gosens, I., Alexeeva, S., Punte, I.M., Versteeg, I., Krieger, E., Neefjes-Mol, C.A., den Hollander, A.I., Letteboer, S.J., Klooster, J. *et al*. (2005) MPP5 recruits MPP4 to the CRB1 complex in photoreceptors. *Invest. Ophthalmol. Vis. Sci.*, **46**, 2192–2201.
10. Aartsen, W.M., Kantardzhieva, A., Klooster, J., van Rossum, A.G., van de Pavert, S.A., Versteeg, I., Cardozo, B.N., Tonagel, F., Beck, S.C., Tanimoto, N. *et al*. (2006) Mpp4 recruits Psd95 and Veli3 towards the photoreceptor synapse. *Hum. Mol. Genet.*, **15**, 1291–1302.
11. Krizaj, D., Demarco, S.J., Johnson, J., Strehler, E.E. and Copenhagen, D.R. (2002) Cell-specific expression of plasma membrane calcium ATPase isoforms in retinal neurons. *J. Comp. Neurol.*, **451**, 1–21.
12. Duncan, J.L., Yang, H., Doan, T., Silverstein, R.S., Murphy, G.J., Nune, G., Liu, X., Copenhagen, D., Tempel, B.L., Rieke, F. *et al*. (2006) Scotopic visual signaling in the mouse retina is modulated by high-affinity plasma membrane calcium extrusion. *J. Neurosci.*, **26**, 7201–7211.
13. Kim, E., DeMarco, S.J., Marfatia, S.M., Chishti, A.H., Sheng, M. and Strehler, E.E. (1998) Plasma membrane Ca2+ ATPase isoform 4b binds to membrane-associated guanylate kinase (MAGUK) proteins via their PDZ (PSD-95/Dlg/ZO-1) domains. *J. Biol. Chem.*, **273**, 1591–1595.
14. Nachman-Clewner, M., St Jules, R. and Townes-Anderson, E. (1999) L-type calcium channels in the photoreceptor ribbon synapse: localization and role in plasticity. *J. Comp. Neurol.*, **415**, 1–16.
15. Krizaj, D. (2005) Serca isoform expression in the mammalian retina. *Exp. Eye. Res.*, **81**, 690–699.
16. Krizaj, D., Lai, F.A. and Copenhagen, D.R. (2003) Ryanodine stores and calcium regulation in the inner segments of salamander rods and cones. *J. Physiol.*, **547**, 761–774.
17. Peng, Y.W., Sharp, A.H., Snyder, S.H. and Yau, K.W. (1991) Localization of the inositol 1,4,5-trisphosphate receptor in synaptic terminals in the vertebrate retina. *Neuron*, **6**, 525–531.
18. Morgans, C.W., Bayley, P.R., Oesch, N.W., Ren, G., Akileswaran, L. and Taylor, W.R. (2005) Photoreceptor calcium channels: insight from night blindness. *Vis. Neurosci.*, **22**, 561–568.
19. Chang, B., Hawes, N.L., Hurd, R.E., Davisson, M.T., Nusinowitz, S. and Heckenlively, J.R. (2002) Retinal degeneration mutants in the mouse. *Vis. Res.*, **42**, 517–525.
20. Mansergh, F., Orton, N.C., Vessey, J.P., Lalonde, M.R., Stell, W.K., Tremblay, F., Barnes, S., Rancourt, D.E. and Bech-Hansen, N.T. (2005) Mutation of the calcium channel gene Cacna1f disrupts calcium signaling, synaptic transmission and cellular organization in mouse retina. *Hum. Mol. Genet.*, **14**, 3035–3046.
21. Haeseleer, F., Imanishi, Y., Maeda, T., Possin, D.E., Maeda, A., Lee, A., Rieke, F. and Palczewski, K. (2004) Essential role of Ca2 + -binding protein 4, a Cav1.4 channel regulator, in photoreceptor synaptic function. *Nat. Neurosci.*, **7**, 1079–1087.
22. Dick, O., tom Dieck, S., Altrock, W.D., Ammermuller, J., Weiler, R., Garner, C.C., Gundelfinger, E.D. and Brandstatter, J.H. (2003) The presynaptic active zone protein bassoon is essential for photoreceptor ribbon synapse formation in the retina. *Neuron*, **37**, 775–786.
23. Tom Dieck, S., Altrock, W.D., Kessels, M.M., Qualmann, B., Regus, H., Brauner, D., Fejtova, A., Bracko, O., Gundelfinger, E.D. and Brandstatter, J.H. (2005) Molecular dissection of the photoreceptor ribbon synapse: physical interaction of Bassoon and RIBEYE is essential for the assembly of the ribbon complex. *J. Cell. Biol.*, **168**, 825–836.
24. Spiwoks-Becker, I., Glas, M., Lasarzik, I. and Vollrath, L. (2004) Mouse photoreceptor synaptic ribbons lose and regain material in response to illumination changes. *Eur. J. Neurosci.*, **19**, 1559–1571.
25. Breton, M.E., Schueller, A.W., Lamb, T.D. and Pugh, E.N., Jr. (1994) Analysis of ERG a-wave amplification and kinetics in terms of the G-protein cascade of phototransduction. *Invest. Ophthalmol. Vis. Sci.*, **35**, 295–309.
26. Krizaj, D. and Copenhagen, D.R. (1998) Compartmentalization of calcium extrusion mechanisms in the outer and inner segments of photoreceptors. *Neuron*, **21**, 249–256.
27. Ruether, K., Grosse, J., Matthiessen, E., Hoffmann, K. and Hartmann, C. (2000) Abnormalities of the photoreceptor-bipolar cell synapse in a substrain of C57BL/10 mice. *Invest. Ophthalmol. Vis. Sci.*, **41**, 4039–4047.
28. Wycisk, K.A., Budde, B., Feil, S., Skosyrski, S., Buzzi, F., Neidhardt, J., Glaus, E., Nurnberg, P., Ruether, K. and Berger, W. (2006) Structural and functional abnormalities of retinal ribbon synapses due to Cacna2d4 mutation. *Invest. Ophthalmol. Vis. Sci.*, **47**, 3523–3530.
29. Verkhratsky, A. (2005) Physiology and pathophysiology of the calcium store in the endoplasmic reticulum of neurons. *Physiol. Rev.*, **85**, 201–279.
30. Chang, B., Heckenlively, J.R., Bayley, P.R., Brecha, N.C., Davisson, M.T., Hawes, N.L., Hirano, A.A., Hurd, R.E., Ikeda, A., Johnson, B.A. *et al*. (2006) The nob2 mouse, a null mutation in Cacna1f: anatomical and functional abnormalities in the outer retina and their consequences on ganglion cell visual responses. *Vis. Neurosci.*, **23**, 11–24.
31. Ball, S.L., Powers, P.A., Shin, H.S., Morgans, C.W., Peachey, N.S. and Gregg, R.G. (2002) Role of the beta(2) subunit of voltage-dependent calcium channels in the retinal outer plexiform layer. *Invest. Ophthalmol. Vis. Sci.*, **43**, 1595–1603.
32. Masu, M., Iwakabe, H., Tagawa, Y., Miyoshi, T., Yamashita, M., Fukuda, Y., Sasaki, H., Hiroi, K., Nakamura, Y., Shigemoto, R. *et al*. (1995) Specific deficit of the ON response in visual transmission by targeted disruption of the mGluR6 gene. *Cell*, **80**, 757–765.
33. Weber, B.H., Schrewe, H., Molday, L.L., Gehrig, A., White, K.L., Seeliger, M.W., Jaissle, G.B., Friedburg, C., Tamm, E. and Molday, R.S. (2002) Inactivation of the murine X-linked juvenile retinoschisis gene, Rs1 h, suggests a role of retinoschisin in retinal cell layer organization and synaptic structure. *Proc. Natl. Acad. Sci. USA*, **99**, 6222–6227.
34. Dhingra, A., Lyubarsky, A., Jiang, M., Pugh, E.N., Jr., Birnbaumer, L., Sterling, P. and Vardi, N. (2000) The light response of ON bipolar neurons requires G[alpha]o. *J. Neurosci.*, **20**, 9053–9058.
35. Pardue, M.T., McCall, M.A., LaVail, M.M., Gregg, R.G. and Peachey, N.S. (1998) A naturally occurring mouse model of X-linked congenital stationary night blindness. *Invest. Ophthalmol. Vis. Sci.*, **39**, 2443–2449.
36. Yang, J., Liu, X., Yue, G., Adamian, M., Bulgakov, O. and Li, T. (2002) Rootletin, a novel coiled-coil protein, is a structural component of the ciliary rootlet. *J. Cell. Biol.*, **159**, 431–440.
37. Makino, C.L., Wen, X.H., Michaud, N., Peshenko, I.V., Pawlyk, B., Brush, R.S., Soloviev, M., Liu, X., Woodruff, M.L., Calvert, P.D. *et al*. (2006) Effects of low AIPL1 expression on phototransduction in rods. *Invest. Ophthalmol. Vis. Sci.*, **47**, 2185–2194.
38. Balkema, G.W., Cusick, K. and Nguyen, T.H. (2001) Diurnal variation in synaptic ribbon length and visual threshold. *Vis. Neurosci.*, **18**, 789–797.
39. Adly, M.A., Spiwoks-Becker, I. and Vollrath, L. (1999) Ultrastructural changes of photoreceptor synaptic ribbons in relation to time of day and illumination. *Invest. Ophthalmol. Vis. Sci.*, **40**, 2165–2172.
40. Li, T., Sandberg, M.A., Pawlyk, B.S., Rosner, B., Hayes, K.C., Dryja, T.P. and Berson, E.L. (1998) Effect of vitamin A supplementation on

rhodopsin mutants threonine-17 –> methionine and proline-347 –> serine in transgenic mice and in cell cultures. *Proc. Natl. Acad. Sci.*, **95**, 11933–11938.
41. Sandberg, M.A., Lee, H., Matthews, G.P. and Gaudio, A.R. (1991) Relationship of oscillatory potential amplitude to A-wave slope over a range of flash luminances in normal subjects. *Invest. Ophthalmol. Vis. Sci.*, **32**, 1508–1516.
42. Liu, X., Bulgakov, O.V., Wen, X.H., Woodruff, M.L., Pawlyk, B., Yang, J., Fain, G.L., Sandberg, M.A., Makino, C.L. and Li, T. (2004) AIPL1, the protein that is defective in Leber congenital amaurosis, is essential for the biosynthesis of retinal rod cGMP phosphodiesterase. *Proc. Natl. Acad. Sci. USA*, **101**, 13903–13908.
43. Yau, K.W. and Nakatani, K. (1984) Electrogenic Na-Ca exchange in retinal rod outer segment. *Nature*, **311**, 661–663.
44. Pepperberg, D.R., Cornwall, M.C., Kahlert, M., Hofmann, K.P., Jin, J., Jones, G.J. and Ripps, H. (1992) Light-dependent delay in the falling phase of the retinal rod photoresponse. *Vis. Neurosci.*, **8**, 9–18.
45. Nikonov, S., Engheta, N. and Pugh, E.N., Jr. (1998) Kinetics of recovery of the dark-adapted salamander rod photoresponse. *J. Gen. Physiol.*, **111**, 7–37.
46. Krispel, C.M., Chen, D., Melling, N., Chen, Y.J., Martemyanov, K.A., Quillinan, N., Arshavsky, V.Y., Wensel, T.G., Chen, C.K. and Burns, M.E. (2006) RGS expression rate-limits recovery of rod photoresponses. *Neuron*, **51**, 409–416.